An Indoor Microwave Radiometer for Measurement of Tropospheric Water

Wenyue Wang, Axel Murk, Eric Sauvageat, Wenzhi Fan, Christoph Dätwyler, Maxime Hervo, Alexander Haefele, and Klemens Hocke

***Abstract*— This article presents the first detailed description of the innovative measurement setup of an indoor tropospheric microwave radiometer [TROpospheric WAter RAdiometer (TROWARA)] that avoids water films on radome. We discuss the performance of a commercial outdoor microwave radiometer [Humidity And Temperature PROfiler radiometer (HATPRO)] for measuring tropospheric water parameters in Bern, Switzerland. The HATPRO is less than 20 m from the TROWARA and has different instrument characteristics. Brightness temperatures measured by HATPRO are analyzed by comparing them with coincident measurements from TROWARA and Radiative Transfer Simulations based on the [European Centre for Medium-Range Weather Forecasts (ECMWF)] operational analysis data (denoted as RTSE). To find the source of brightness temperature bias, a gradient boosting decision tree is used to analyze the sensitivity of eight feature factors to bias. Data processing routines of the two radiometers use different algorithms to retrieve integrated water vapor (IWV) and integrated cloud liquid water (ILW), whereas the same physical algorithms based on the radiative transfer equation are applied to obtain the opacity and rain rate. Using 62 days of data with varied weather conditions, it was found that TROWARA brightness temperatures are in good agreement with RTSE. HATPRO brightness temperatures are significantly overestimated by about 5 K at 22 GHz, compared to TROWARA and RTSE. HATPRO brightness temperatures at 31 GHz agree well with TROWARA and RTSE (within about ±1 K). The overestimated brightness temperatures in the K-band and the HATPRO retrieval algorithm lead to an overestimation of IWV and ILW by HATPRO. The opacities at 31 GHz match very well for TROWARA and HATPRO during no rain with a verified R^2 of 0.96. However, liquid water floating or remaining water films on the radome of the outdoor HATPRO radiometer induce an overestimation of the rain rate. The physical reason for the overestimated 22-GHz brightness temperatures of the HATPRO is mainly the result of the combined effect of instrument calibration, the surrounding environment of the instrument, and the Sun elevation angle. This can be a problem with the Generation 2 HATPRO radiometer and this problem was resolved in the Generation 5 HATPRO radiometer.**

***Index Terms*— Atmospheric Radiative Transfer Simulator (ARTS), brightness temperature, European Centre for Medium-Range Weather Forecasts (ECMWF), gradient boosting decision tree (GBDT), Humidity And Temperature PROfiler radiometer (HATPRO), K-band, microwave radiometer, radiometer technology, rain rate, remote sensing, water films, water vapor.**

I. Introduction

ACCURATE measurements of tropospheric water (e.g., water vapor, cloud, and rain) are required for studies of climate change. Water vapor is the most abundant greenhouse gas [1]. Clouds affect the Earth's radiation budget, and any subtle change in cloud properties can alter climate responses to anthropogenic aerosols or other factors associated with global change [2]. Heavy rainfall often causes flooding [3]. The advantages of ground-based microwave radiometers in the K-band (21.3–31.5 GHz) for measuring atmospheric water are well known: continuous, automatic operation with high time resolution in almost all weather conditions, day and night [4], [5]. Bernet et al. [6] showed that ground-based microwave radiometry is adequate to monitor long-term trends of integrated water vapor (IWV). Ground-based microwave radiometers are further important for cross validation of satellite measurements of IWV [7], [8]. Compared to ground-based global navigation satellite system (GNSS) receivers, a radiometer can provide IWV with a higher temporal and horizontal resolution (e.g., 10 s and 100 m). Thus, a ground-based radiometer can achieve a high coincidence with an overhead satellite observation of IWV, which is of interest for the study of the small-scale variability of IWV [9]. Exploring measurement capabilities of ground-based microwave radiometers and analyzing biases and uncertainties in atmospheric water retrievals are therefore necessary.

Microwave radiometers measure brightness temperatures (Tb) to derive atmospheric water parameters, including IWV, integrated cloud liquid water (ILW), and rain rate. To evaluate the reliability of the derived IWV, it is often compared to water vapor derived from other techniques such as radiosonde, GNSS, Fourier transform infrared spectrometer (FTIR), and Raman lidar [6], [10], [11]. Radiosondes cannot directly observe the characteristics of the cloud liquid [2]. In situ measurements of ILW can provide the most accurate microphysical information on clouds [12], but it requires aircraft to traverse

Manuscript received 23 November 2022; revised 21 February 2023; accepted 21 March 2023. Date of publication 23 March 2023; date of current version 4 April 2023. The work of Wenyue Wang was supported in part by the China Scholarship Council (CSC), in part by the Global Climate Observing System (GCOS Switzerland) Project "Operational Monitoring of the Rain Rate by Ground-based Microwave Radiometry in Switzerland", and in part by the Aerosol, Clouds and Trace Gases Research Infrastructure (ACTRIS). *(Corresponding author: Wenyue Wang.)*

Wenyue Wang, Axel Murk, Eric Sauvageat, Christoph Dätwyler, and Klemens Hocke are with the Institute of Applied Physics and the Oeschger Centre for Climate Change Research, University of Bern, 3012 Bern, Switzerland (e-mail: wenyue.wang@unibe.ch; axel.murk@unibe.ch; eric.sauvageat@unibe.ch; christoph.daetwyler@unibe.ch; klemens.hocke@unibe.ch).

Wenzhi Fan is with the School of Earth and Space Sciences, Peking University, Beijing 100084, China (e-mail: wenzhi.fan@pku.edu.cn).

Maxime Hervo and Alexander Haefele are with the Federal Office of Meteorology and Climatology, MeteoSwiss, 1530 Payerne, Switzerland (e-mail: maxime.hervo@meteoswiss.ch; alexander.haefele@meteoswiss.ch).

Digital Object Identifier 10.1109/TGRS.2023.3261067

rapidly evolving clouds and cannot represent radiometer sampling [13]. The vertical reflectivity of expensive and sparsely distributed cloud radar is more suitable for obtaining ILW with small droplets [14]. Rain rates are primarily verified by the accumulated rain measured by rain gauges with a coarser time resolution compared to radiometers. The intercomparison of two microwave radiometers with a different setup is undoubtedly a good choice because they have the same observation principle, which helps to account for various sources of error. The Humidity And Temperature PROfiler (HATPRO) radiometer manufactured by Radiometer Physics GmbH (RPG) is widely used for meteorological monitoring and forecasting networks worldwide [15]. The TROpospheric WAter RAdiometer (TROWARA) built and operated by the Institute of Applied Physics (IAP) at the University of Bern, Bern, Switzerland, has been operational for 28 years. Many studies have compared it to global positioning system (GPS), in situ instruments, and reanalysis data and demonstrated TROWARA's superior ability to retrieve atmospheric water, especially IWV [16], [17], [18], [19].

Cimini et al. [20] evaluated the agreement of Tb measured by two ground-based microwave radiometers during the Temperature, hUmidity, and Cloud (TUC) profiling campaign. Mattioli et al. [21] explored the scanning capabilities of three microwave radiometers and their monitoring of IWV and ILW during the 2003 Cloudiness Inter-Comparison Experiment. Mattioli et al. [22] compared Tb calculated by radiosonde with those measured by three microwave radiometers at 23.8 and 31.4 GHz as well as the IWV from the radiometers and a GPS station. However, these studies lack an analysis of the problems of radiometers due to outdoor operation. Microwave radiation strongly emitted and scattered by rainwater on the radome affects the radiometric signal, making it difficult to identify the signal of raindrops in the air and other atmospheric parameters. This leads to a decrease in the accuracy of the atmospheric Tb measurements and parameter retrievals from ground-based microwave radiometers [23], [24]. Instrument hardware upgrades can reduce the water film bias [25], but even with blowers and hydrophobic materials, rainwater is still likely to float or remain on the radome during and after rain [26]. Indoor observations can effectively avoid radome and antenna wetting, so a comparison of indoor and outdoor radiometers can reveal possible differences in Tb, opacity, IWV, rain rate, and other atmospheric parameters, which are caused by undesired water films on the outdoor radiometer radome. TROWARA is the only indoor microwave radiometer to our knowledge for the measurement of tropospheric water parameters during rain and no rain, which is mentioned in the literature (e.g., [6]). Thus, this present article includes the details of the measurement setup of TROWARA, which are useful for the installation of indoor radiometers at other locations in the world.

This article is organized as follows. Section II describes the study site and instrumentation. Section III outlines the principle and feature selection of the gradient boosting decision tree (GBDT) and methodologies for IWV, ILW, and rain rate retrievals. Section IV presents brightness temperature, opacity, and atmospheric water parameters comparisons in the K-band for the 62 days of coincident measurements. The brightness temperature bias for the two radiometers and the effect of liquid water on the radome of an outdoor radiometer are also discussed in this section. Conclusions are given in Section V.

II. Instrumentation

The HATPRO (HATPRO-G2) microwave radiometer was operated in Payerne (46.82°N, 6.95°E; 491 m asl) from 2009 to 2021 by the Swiss Federal Institute of Meteorology and Climatology (MeteoSwiss). The instrument was moved in November 2021 from Payerne to the roof of the ExWi building (46.95°N, 7.44°E; Alt. 575 m asl) at the University of Bern for an intercomparison between the outdoor radiometer HATPRO and the indoor radiometer TROWARA. This study assesses the brightness temperature (Tb), opacity, and the retrieval products IWV, ILW, and rain rates from December 1, 2021 to January 31, 2022. In addition, the Tb of the two instruments is also compared with the Tb simulations (RTSE Tb) based on calculations of the Atmospheric Radiative Transfer Simulator (ARTS) using the daily operational analysis data of the European Centre for Medium-Range Weather Forecasts (ECMWF). The temporal and spatial resolutions of ECMWF are 6 h and 1.125°, respectively. By using the data of the ExWi weather station, the ECMWF profiles from about 1.1 to 70 km asl are linearly extrapolated to the surface at 0.575 km asl. ARTS is a radiative transfer model focused on the microwave frequency range [27]. Inputs to the model include pressure, height, temperature, and water vapor density. H_2O, O_2, and N_2 concentrations are used to calculate the absorption coefficients over a range of microwave frequencies and simulate the emission spectrum at the location of the instruments. We do not consider hydrometeors or other aerosols in the simulation so that the modeled brightness temperature is only accurate during clear-sky periods. The outdoor HATPRO and the indoor TROWARA radiometer conduct parallel observations from locations less than 20 m apart at the same azimuth and elevation angle, 130° (southeast) and 40°, respectively.

A. Indoor Radiometer TROWARA

The TROWARA radiometer has been operated by the IAP since 1994 on the roof of the University of Bern. This instrument measures the brightness temperatures at three microwave frequency channels with a time resolution of 7 s. Two microwave channels are at frequencies of 21.385 GHz (bandwidth = 100 MHz) and 31.5 GHz (bandwidth = 200 MHz), and the third channel built in November 2007 is 22.235 GHz (bandwidth = 400 MHz). The 22.235-GHz channel is located in the center of the water vapor line and is more sensitive to microwave emission from atmospheric water vapor than the 21.385-GHz channel. The 31.5-GHz channel is more sensitive to microwave emission from atmospheric liquid water than the other two channels. The half-power beamwidth of TROWARA antenna beams is 4° for all frequencies. TROWARA also includes an additional thermal infrared channel at 9.5–11.5 μm. TROWARA can provide accurate

IWV, ILW, and high-quality rain rate values using opacity-based physical retrieval algorithms [19], [28]. A standard weather station called ExWi Weather Station is also operated on the ExWi building, a few meters away from TROWARA, to provide weather information and auxiliary data for the retrieval models.

TROWARA was on the roof outdoors from 1994 to April 2002. The disadvantages of its outdoor operation are twofold: 1) the temperature of the radiometer body was unstable due to solar heating and 2) rain collected on the radiometer radome caused unreliable measurements for up to several hours after rainfall. TROWARA was moved from outdoor to indoor constant temperature laboratory and was reinstalled in November 2002 [29] [Fig. 1(a)]. The antenna receives atmospheric radiation through a microwave transparent window that is well protected against rain by a wall overhang [Fig. 1(b)]. The window only can get wet in case of strong southeasterly winds that are very rare during rain events in Bern. This indoor operation avoids contamination of measurements caused by antenna wetness and allows TROWARA to measure even on rainy days. Generally, the stability and accuracy of TROWARA's measurements of IWV and ILW strongly increased after TROWARA became an indoor radiometer in 2002, and the rain rate retrieval is not biased by water films on the radome.

The original design and construction of TROWARA are described by Peter and Kämpfer [30]. Scientists and engineers from the IAP at the University of Bern improved TROWARA and enabled TROWARA to measure continuously without break points in the IWV time series since 2002. The amount of data gaps after 2002 is less than 2%. The latest block diagram of TROWARA is shown in Fig. 2. The developed radiometer model provides a good estimate of the antenna temperature by measuring the reflection and transmission coefficients of all radiometer components and enables automatic internal calibration at fairly small time intervals [29]. The active cold loads (ACLs) replaced cooled cold loads in 2004, and two ferrite switches for each frequency switch between the antenna, the ACL, and a matched waveguide termination, which is used as hot load [31]. TROWARA is calibrated with the ACL and hot load. The ACL temperature is determined by the manual tipping calibration using clear-sky brightness temperatures at different antenna elevation angles between 20° and 45°. Because of the high stability of TROWARA, only two tipping curve calibrations are required per year.

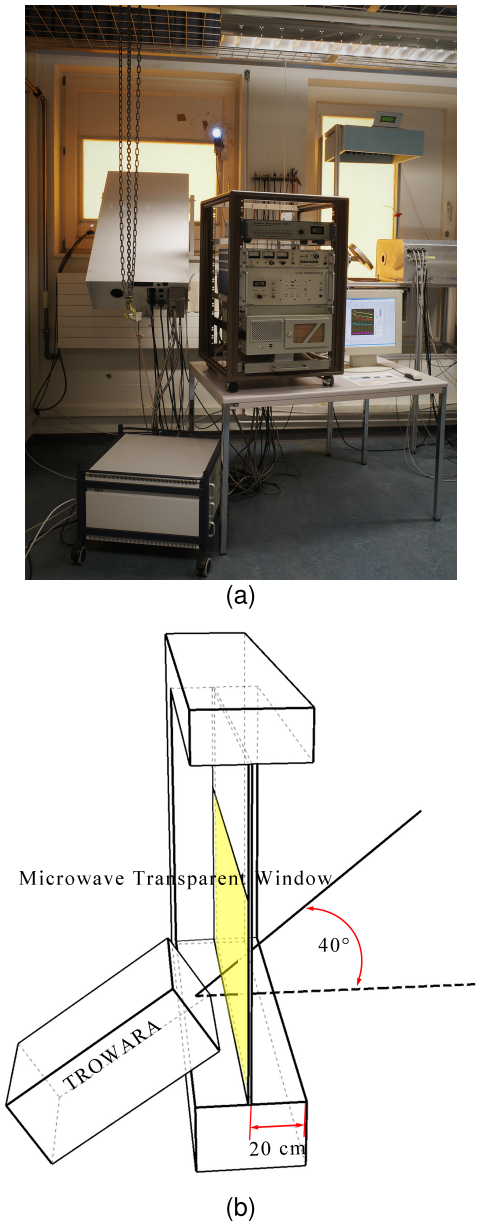

Fig. 1. (a) TROWARA in an indoor laboratory on the ExWi roof. (b) Measurement geometry of TROWARA observing the sky through a yellow microwave transparent window.

B. Outdoor Radiometer HATPRO

The HATPRO Generation 2 (G2) is a ground-based dual-polarization radiometer (R-DPR-09/016) manufactured in 2009 with a time resolution of 1–2 s. This instrument measures microwave radiances (brightness temperatures) at 14 frequencies. Seven microwave channels in the water vapor band (K-band) 22.24, 23.04, 23.84, 25.44, 26.24, 27.84, and 31.4 GHz provide atmospheric humidity and cloud liquid water content in the troposphere, and their bandwidth is between 0.1 and 2 GHz. Another seven channels in the oxygen band (V-band) from 51 to 58 GHz are used to determine atmospheric temperature properties [32]. The half-power beamwidth of HATPRO antenna beams is 3.5° for K-band frequencies. HATPRO also includes a GPS for instrument location and observation time. HATPRO can retrieve IWV and ILW using quadratic regression (QR) with software provided by the HATPRO instrument manufacturer. The radiometer has additional surface sensors to observe weather parameters such as temperature, pressure, and relative humidity. These sensors also provide input data for retrieval models. The complete HATPRO instrument and software descriptions can be found on the RPG website [33].

Generation 2 HATPRO (HATPRO G2) achieves thermal stabilization through a dual-stage thermal control system consisting of a main cooler followed by a Peltier stage for the receivers [26]. The operating environment of its receiver is in the temperature range of −30 °C to 40 °C. The antenna of the

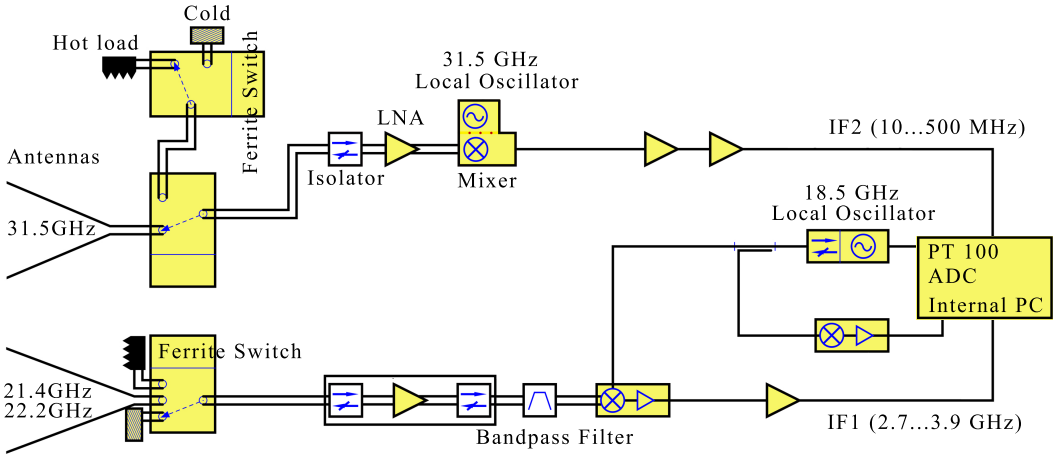

Fig. 2. Block diagram of TROWARA operating at 21.4, 22.2, and 31.5 GHz. The instrument is calibrated using two ferrite circulator switches to switch between the lens antennas, an ambient temperature load, and an ACL with an effective temperature in the order of 120 K.

outdoor HATPRO receives atmospheric radiation through the microwave transparent foil (radome). Hydrophobic material radome and radial blower prevent or reduce the water film on the radome during rain. The rain detector of the HATPRO and software-defined humidity threshold automatically control the speed of the blower.

HATPRO performs absolute calibration using a liquid nitrogen-cooled load mounted externally to the radiometer box and an internal blackbody load at ambient temperature as targets [34]. During calibration, an internal scanning mirror keeps the antenna pointed at each target, and the HATPRO software automatically corrects for calibration errors due to microwave reflections from the liquid nitrogen-air interface. One built-in diode noise source for each receiver replaces the liquid nitrogen-cooled load, enabling automatic internal calibration of the HATPRO [26]. For low atmospheric opacity (high transparency) channels, HATPRO G2 also has an option of tipping curve calibration [35], which is not enabled for the radiometer on site.

III. Methodology

A. Gradient Boosting Decision Tree

It is considered to be one of the best performing ensemble learning methods in machine learning. GBDT uses the negative gradient of the loss function to fit the residual of the previous round of base learners so that the residual estimate of each round gradually decreases close to the actual value [36]. GBDT improves the generalization ability and robustness of a single model and has an interpretable regression procedure.

An advantage of GBDT is that the relative importance of the features used by the model can be output after model training, which is often used for feature selection to understand which factors have a key impact on prediction [37]. Friedman [38] proposed the computation of GBDT feature selection. The basic idea is that the average selection frequency J_j of the feature j serves as a statistic to measure its importance. The more times an input feature is selected as a branch feature during branching in a regression tree, the more important the feature is. The number of times is normalized to the relative frequency, and then, the selected frequencies of the input features in all regression trees are averaged

$$\hat{J}_j^2 = \frac{1}{M}\sum_{m=1}^{M} \hat{J}_j^2(T_m) \tag{1}$$

where M is the number of trees and $m = 1, 2, \ldots, M$. The importance of feature j for a decision tree T is given as follows:

$$\hat{J}_j^2(T) = \sum_{t=1}^{L-1} \hat{i}_t^2 1(v_t = j). \tag{2}$$

Here, it is assumed that every tree is binary tree, so L is the number of terminal nodes and $L-1$ is the number of nonterminal nodes. v_t is the splitting variable associated with node t, and i_t^2 is the square of loss reduction after node t splits.

B. IWV and ILW Retrieval

TROWARA uses the two microwave frequencies 21.385 and 31.5 GHz to retrieve IWV and integrated liquid water (ILW). The following is a brief explanation of the retrieval technique. It is assumed that there is a plane-parallel atmosphere, so the radiative transfer equation for nonscattering atmospheres is

$$\mathrm{Tb}_f = \mathrm{Tb}_c \cdot e^{-\tau_f/\mu} + \mathrm{Tm}_f \cdot \left(1 - e^{-\tau_f/\mu}\right) \tag{3}$$

where τ_f is the zenith opacity of the atmosphere. μ is the cosine of the zenith angle θ, i.e., $\mu = \cos\theta$. Tb_f is the brightness temperature observed by TROWARA, and Tb_c is the brightness temperature of the cosmic microwave background. Tm_f is the effective mean temperature of the troposphere calculated by the linear equation of surface temperature, pressure, and relative humidity. It is also frequency (and site) dependent.

Equation (3) derives the zenith opacity as

$$\tau_f = -\mu \cdot \ln\left(\frac{\mathrm{Tm}_f - \mathrm{Tb}_f}{\mathrm{Tm}_f - \mathrm{Tb}_c}\right). \tag{4}$$

Equation (4) can also be expressed as a linear combination of IWV, ILW, and integrated rain liquid (IRL), where ILW

is the integrated liquid water of the cloud droplets along the zenith direction. Ice and dry snow contribute negligibly to radiation because of their small dielectric losses

$$\tau_f = (a_f + b_f \cdot \mathrm{IWV} + c_f \cdot \mathrm{ILW}) + \tau_{\mathrm{rf}} \tag{5}$$

$$\tau_{\mathrm{rf}} = c_f \cdot G_{M,f} \cdot \mathrm{IRL} \tag{6}$$

where the coefficients a_f and b_f depend on air pressure. They can be statistically obtained from simultaneous measurements of radiosondes and fine-tuned during periods of a clear sky. The coefficient c_f depends on air temperature and frequency. It is the Rayleigh mass absorption coefficient of cloud water, which can be obtained from a dielectric model of water. τ_{rf} is the rain zenith opacity. $G_{M,f}$ is the rain Mie gain.

The retrieval of IWV and ILW uses a physical algorithm for microwave radiometer data during no rainfall ($G_{M,f} = 0$)

$$\mathrm{IWV} = \frac{\tau_{21} - a_{21} - \gamma(\tau_{31} - a_{31})}{b_{21}(1 - \beta\gamma)} \tag{7}$$

$$\mathrm{ILW} = \frac{\tau_{31} - a_{31} - \beta(\tau_{21} - a_{21})}{c_{31}(1 - \beta\gamma)} \tag{8}$$

where subscripts 21 and 31 represent the microwave frequencies of TROWARA at 21.385 and 31.5 GHz, respectively. $\beta = b_{31}/b_{21} < 0.5$, and $\gamma = c_{21}/c_{31} \cong 0.5$. Details of TROWARA's IWV and ILW retrieval algorithms are described by Mätzler and Morland [28].

HATPRO G2 uses the seven K-band microwave frequencies to retrieve IWV and ILW based on the QR method. The QR retrieval technique can be described as

$$\mathrm{Out}_n = \mathrm{Os}_n + \sum_{\text{sensors}} \mathrm{ML}_{ns} \cdot \mathrm{Mr}_s + \sum_{\text{sensors}} \mathrm{MQ}_{ns} \cdot \mathrm{Mr}_s^2 + \sum_{\text{freq}} \mathrm{TL}_{nf} \cdot \mathrm{Tb}_f + \sum_{\text{freq}} \mathrm{TQ}_{nf} \cdot \mathrm{Tb}_f^2 \tag{9}$$

where n is the number of retrieval parameters and Out_n is the output parameter (IWV or ILW). Os_n is the retrieval offset for Out_n. s is the number of times to check the surface sensor, and Mr_s is the meteorological parameters temperature, pressure, and relative humidity read by the sensor. ML_{ns} and MQ_{ns} are the linear coefficient and quadratic coefficient of Mr_s, respectively. The subscript f denotes the microwave frequency. Tb_f is the brightness temperature observed by HATPRO. TL_{nf} and TQ_{nf} are the linear coefficient and quadratic coefficient of Tb_f, respectively. These coefficients are derived by RPG based on long-term radiosonde datasets. The limitation is that the retrieval algorithms can only be applied to the range of atmospheric conditions included in their training datasets. More details for the HATPRO retrieval are described in the RPG operation and software guide [26], [39].

C. Rain Rate Retrieval

Because the rain rate retrieval is not included in the standard HATPRO software, in this study, we use the same opacity-based physical method as for TROWARA to retrieve rain rates for HATPRO. During rain, τ_{rf} is determined iteratively. The iterative equation can be expressed as

$$\tau_{\mathrm{rf}}^{(k+1)} = -\mu \cdot \ln\left(\frac{\mathrm{Tm}_{\mathrm{rf}}\left(\tau_{\mathrm{rf}}^{(k)}\right) - \mathrm{Tb}_{\mathrm{rf}}}{\mathrm{Tm}_{\mathrm{rf}}\left(\tau_{\mathrm{rf}}^{(k)}\right) - \mathrm{Tb}_f}\right) \tag{10}$$

where $\tau_{\mathrm{rf}}^{(k+1)}$ is the rain zenith opacity at the kth iteration. $\mathrm{Tm}_{\mathrm{rf}}$ is the effective mean temperature during rain. $\mathrm{Tb}_{\mathrm{rf}}$ is the brightness temperature during rain, and Tb_f is the brightness temperature without rain. Equation (10) basically converges after two iterations.

Rain rate R_f can be calculated from rain zenith opacity

$$R_f = \frac{\tau_{\mathrm{rf}}}{g_{\mathrm{rf}} \cdot \mathrm{Hr}} \tag{11}$$

where g_{rf} is the effective rain absorption coefficient calculated with Mie theory. Hr is the vertical distance from the melting layer to the surface when it rains. The details of the rain rate retrieval algorithm for HATPRO and TROWARA are described by Wang et al. [19].

IV. Results and Discussion

A. Brightness Temperature Comparison

The HATPRO G2 radiometer was transferred from Payerne to Bern in November 2021, and it was calibrated on November 11, 2021. Our study considers the HATPRO observations after December 1, 2021. Fig. 3 shows a two-month Tb time series of the same microwave channels 22 and 31 GHz from HATPRO, TROWARA, and RTSE. The rain flag marks the time of rain. RTSE Tb is missing during rainfall when Tb observed by HATPRO and TROWARA increases remarkably. As shown in Fig. 3(a), RTSE Tb agrees better with TROWARA Tb than HATPRO Tb. The mean value of TROWARA Tb at 22 GHz is around 22 K during no rainfall, and HATPRO Tb is significantly overestimated by more than 5 K. This overestimation can be clearly seen from January 22 to 26 (shaded area). As shown in Fig. 3(b), there is comparatively good agreement between TROWARA Tb, HATPRO Tb, and RTSE Tb. The mean value of TROWARA Tb at 31 GHz is around 17 K during no rainfall, with HATPRO overestimating Tb by around 1 K on average. During rainfall, HATPRO Tb values are significantly higher than TROWARA Tb at both 22 and 31 GHz due to the influence of a water film on the radome, which is described in detail next.

Fig. 4 shows the mean value and standard deviation of Tb of HATPRO and TROWARA in the K-band for three days of dry clear-sky conditions on January 1, 14, and 22, 2022, and RTSE Tb as a function of frequency over the same time period. The mean value of IWV and ILW is about 8.5 and 0 mm, respectively. As shown in Fig. 4(a), TROWARA Tb at microwave frequencies 22 and 31 GHz agrees very well with RTSE Tb, while there is a deviation of 2.5 K between TROWARA and RTSE at 21 GHz. Since TROWARA retrieval coefficients are corrected to match GPS and radiosonde data, the intercomparison of IWV from TROWARA and ERA5 reanalysis only resulted in a small mean difference of 0.38 mm for no rain conditions [40]. Note that the maximum value of the RTSE curve appears to be at 22.5 GHz, while the line

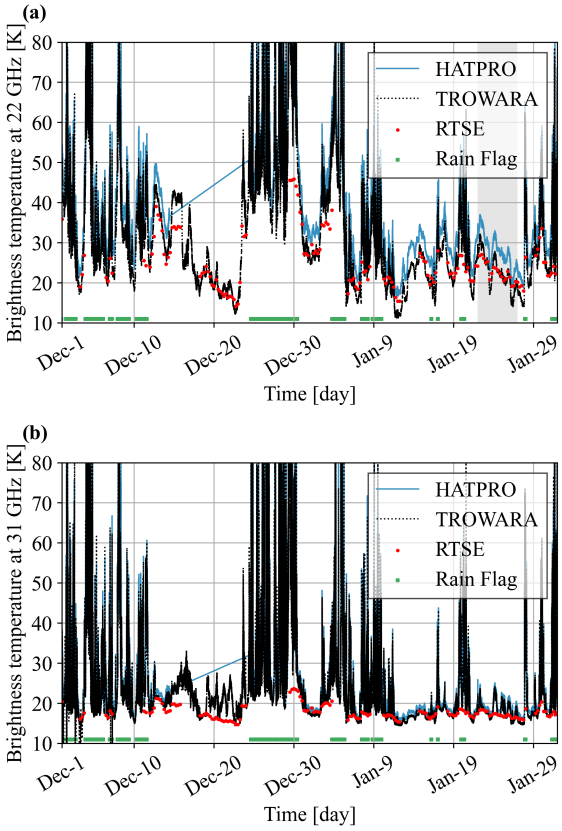

Fig. 3. Time series of the brightness temperature (Tb) observed by HATPRO and TROWARA, as well as radiative transfer simulations based on the operational analysis data ECMWF (RTSE) Tb at (a) 22 and (b) 31 GHz from December 1, 2021 to January 31, 2022. The rain flag data observed by the HATPRO rain detector are used to identify rain. The shaded area is from January 22 to 26, 2022.

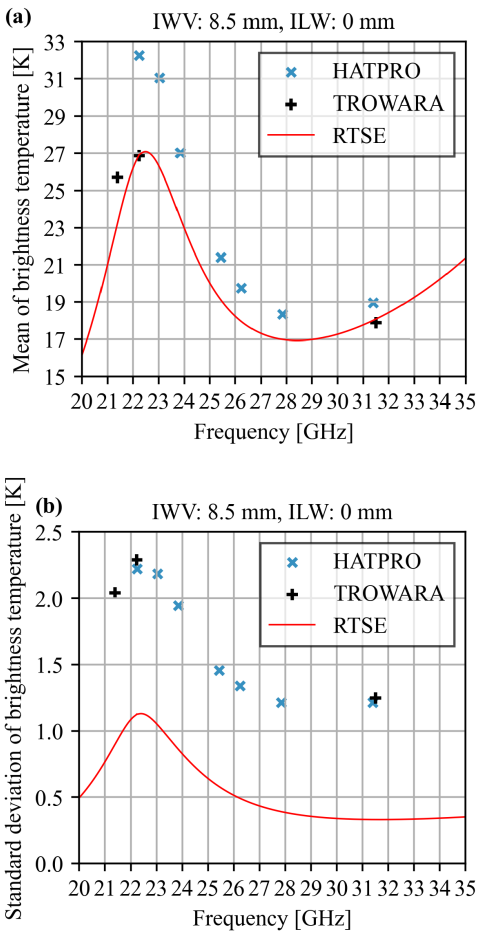

Fig. 4. (a) Mean and (b) standard deviation of Tb observed by HATPRO, TROWARA, as well as RTSE Tb, only for clear conditions (three days).

center of the water vapor line should be at 22.235 GHz. The reason is the high pressure in the troposphere [41]. HATPRO Tb is significantly enhanced at all microwave frequencies. Compared to RTSE Tb, HATPRO Tb has a maximum deviation of 5.3 K at 22 GHz and a minimum deviation of 1.0 K at 31 GHz. As shown in Fig. 4(b), the standard deviations of HATPRO and TROWARA are almost the same at 22 and 31 GHz. This further suggests that the changes of Tb they observed are similar when HATPRO had no water film on the radome under dry conditions.

The effect of common instrument characteristics on brightness temperature is unlikely to be the main reason for the overestimation of HATPRO Tb, such as antenna beamwidth and individual filter bandwidth. The beamwidths of HATPRO and TROWARA are relatively narrow, with half-power beamwidths of 3.5° and 4°, respectively. At an observation elevation angle of 40°, the bias caused by these beamwidths can be negligible in the K-band. Bandwidth errors of microwave channels are less important for K-band. At these frequencies, it is acceptable to use a wider bandwidth to improve detection under low signal-to-noise ratio conditions [42]. It is worth noting that a frequency offset of the channels can lead to a considerable bias.

The HATPRO calibration bias is more likely a cause of the overestimation of HATPRO Tb, including nonlinearities in the calibration transfer characteristics and nonlinear corrections. Rose et al. [26] stated that the HATPRO-G2 is calibrated by noise injection and based on a four-point method to correct the nonlinearities. One possible explanation for the bias is that the coefficients for this correction are incorrect. TROWARA assumes a linear transfer characteristic. It should be less prone to linearity errors since the calibration is done with the ACL and ambient, whereas HATPRO has to extrapolate from ambient and ambient plus noise diode ($\gg$ 300 K) to a sky temperature of 30 K. From 13:00 to 17:00 on September 22, 2022, we performed liquid nitrogen calibration during clear sky for HATPRO. Fig. 5 shows the change in Tb from before to after HATPRO calibration. Before the HATPRO calibration at 22 GHz, the Tb bias between HATPRO and TROWARA is 7.7 K, much higher than the one in January 2022 in Fig. 4. HATPRO calibration reduces the Tb bias, correcting 1.6 K (21%) to 6.1 K. In addition, the small-scale variations of Tb from TROWARA and HATPRO are perfectly correlated. Thus, the variations are real atmospheric variations and not instrument noise. We also checked the pointing accuracy of the two radiometers by scanning the Sun to determine whether there is any bias on the elevation angle that could explain the Tb bias between the two instruments [43] and found that HATPRO has a slightly higher elevation angle than TROWARA. The actual elevation angles of TROWARA and HATPRO determined by the solar drift scans were 40.05° and 41.53°, respectively. The effect of this difference in elevation angle on the Tb bias is

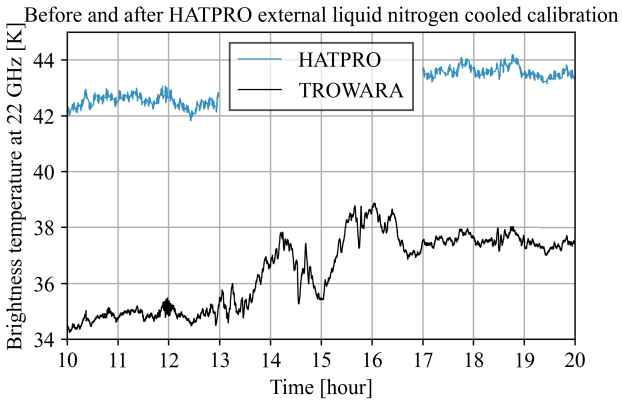

Fig. 5. Time series of Tb observed by HATPRO and TROWARA on September 22, 2022. HATPRO was calibrated with external liquid nitrogen from 13:00 to 17:00, while TROWARA continued to observe.

about −0.68 K during a clear sky in January 2022. Given that it would result in an underestimation of Tb, the pointing bias might compensate partly for HATPRO's other biases (e.g., nonlinearity of calibration).

Before the HATPRO moved to Bern, Hervo et al. [44] in Payerne studied the difference between Tb measured by this HATPRO G2 and a new Generation 5 HATPRO (HATPRO G5) and radiative transfer simulations based on radiosonde data (denoted as RTSR) from March 25 to August 25, 2021. Fig. 6 is taken from their research report. As shown in Fig. 6(a), the Tb bias between HATPRO G5 and RTSR is significantly smaller than the HATPRO G2. HATPRO G2 Tb at 22 GHz in Payerne is overestimated by about 2.19 K at zenith compared to RTSR [Fig. 6(b)]. The overestimation of HATPRO Tb occurs in a different manner in Payerne and Bern due to instrument elevation of 90° in Payerne. An observation elevation angle of 90° produces a lower overestimation than measurements at much lower elevation angles. It may also be due to different weather conditions in these two places.

The feature importance calculation of GBDT can further quantify the sensitivity of multiple factors to the contribution of Tb bias and thus infer the source of the bias [36]. The bias may be caused by a combination of factors, including voltages, channel gain (slope of the linear response), and temperature of ambient blackbody target, which are related to instrument calibration; environmental temperature and environmental relative humidity, which are related to the instrument surrounding environment; receiver temperature and receiver stability, which are related to receiver performance; and Sun elevation angle, which is related to the position of the Sun relative to the instrument and diurnal distribution. These eight factors provided by HATPRO are the input learning datasets for GBDT here. Because TROWARA fits well with RTSE and the lower temporal resolution of RTSE cannot meet machine learning data volume requirements, the difference between the Tb of HATPRO and TROWARA at 22 GHz is marked as the actual value of the bias. More than 280 000 quality control samples in 23 clear-sky days are collected to improve model generalization and prevent overfitting. The training samples and test samples are randomly selected to account for 90% and 10% of the total samples, respectively. The GBDT model parameters set in this study are given as

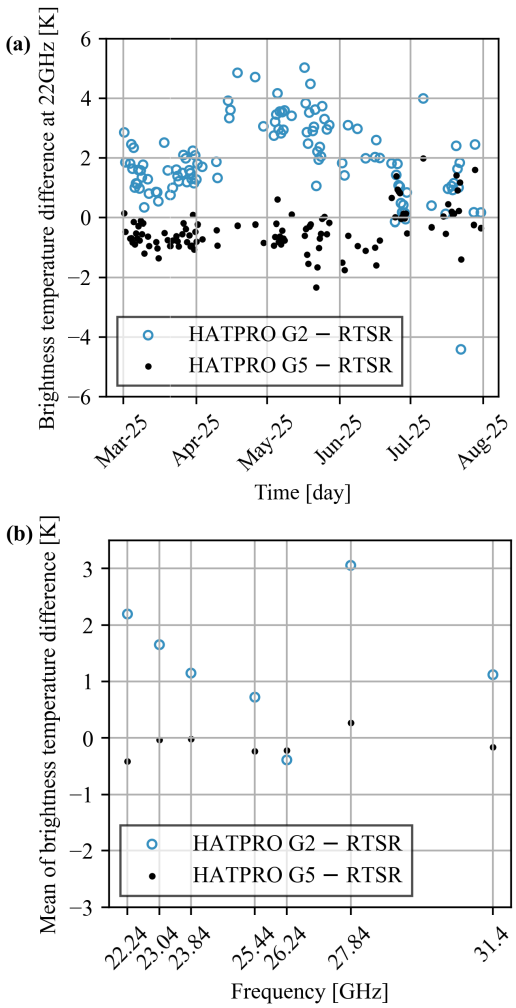

Fig. 6. (a) Difference between brightness temperatures measured by HATPRO G2 and HATPRO G5 and radiative transfer simulations based on radiosonde data (RTSR) at 22 GHz in Payerne. (b) Mean value of the difference in brightness temperature between measurements and simulations at seven K-band frequencies.

follows: the learning rate is 0.07, the subsampling rate is 0.85, the maximum depth of decision tree is 26, the minimum number of samples for leaf nodes is 22, the minimum number of samples for internal nodes is 60, the number of features for optimal segmentation is 2, the number of boosting stages to perform is 1000, and the random state is 10. After training, the GBDT model obtained a coefficient of determination (R^2) of 0.99 and a root-mean-square error (RMSE) of 0.004 K, which means that one or more of these input factors are responsible for the Tb bias. Fig. 7 shows the bias-contribution scores. The top two with high bias-contribution scores are instrument calibration, consisting of temperature of blackbody target, channel gain, and voltages; and instrument surrounding environment, consisting of relative humidity and temperature. The sums of their associated factors are all above 0.37. The Sun elevation angle also has a large bias contribution with a score of 0.21, while the HATPRO receiver performance contributes very little to the Tb bias.

B. Intercomparison of IWV, ILW, Opacity, and Rain Rate

Fig. 8 shows a two-month time series and a scatter plot of HATPRO IWV and TROWARA IWV retrieved by (7) and (9),

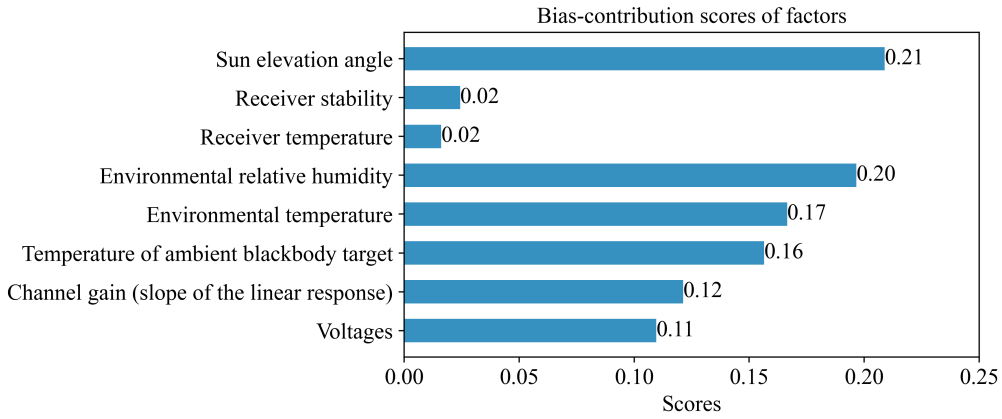

Fig. 7. Contribution of factors to the Tb bias at 22 GHz using the GBDT method.

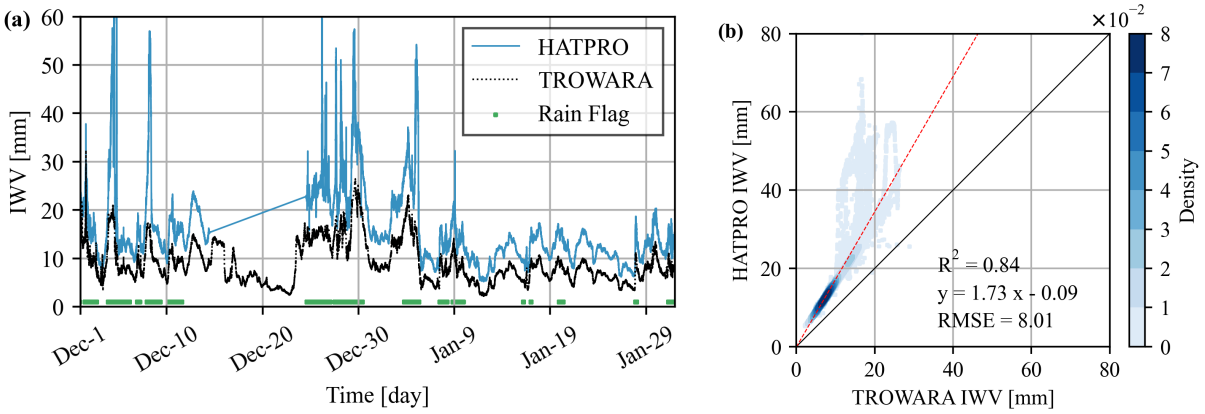

Fig. 8. (a) Time series of the IWV provided by HATPRO and TROWARA from December 1, 2021 to January 31, 2022. The rain flag data observed by the HATPRO rain detector are used to identify rain. (b) Scatter plot of IWV provided by HATPRO and TROWARA from December 1, 2021 to January 31, 2022. The black solid line is the 1:1 line, and the red dashed line is the linear regression fit line. The blue gradient represents the density of the scatter distribution calculated by the Gaussian kernel.

respectively. Note that the IWV during rain is not provided by TROWARA, but obtained by interpolating the opacity before and after rain. This interpolation of the TROWARA retrieval is useful to study the variation of IWV during rain [3], [40]. As shown in Fig. 8(a), during no rainfall, the mean value of TROWARA IWV is around 7 mm. TROWARA IWV values are higher during rainfall than during no rainfall. Hocke et al. [40] showed that TROWARA IWV agrees with GNSS IWV and ERA5 IWV even during rain conditions. During no rainfall, the mean value of HATPRO IWV is around 11 mm. HATPRO IWV increases dramatically during rainfall. As shown in Fig. 8(b), HATPRO IWV is significantly overestimated compared to TROWARA IWV. The slope and intercept of the linear fit are 1.73 and −0.09 mm, respectively. The area with the minimum distribution density (light blue area) corresponds to large values of HATPRO IWV, and the linear regression fit line is located above the 1:1 line. The overestimation of IWV by this HATPRO also occurred in the measurements in Payerne. Hocke et al. [40] intended to present a comparison between IWV obtained by radiosonde, GNSS, ERA5, and HATPRO at Payerne. However, they excluded the HATPRO G2 from this intercomparison because of its too strong positive deviations compared to the other three sources. TROWARA IWV and HATPRO IWV also present similar variations. The R^2 and RMSE between TROWARA and HATPRO IWV are 0.84 and 8.01 mm, respectively.

Fig. 9 shows a two-month time series and a scatter plot of TROWARA ILW and HATPRO ILW retrieved by (8) and (9), respectively. As shown in Fig. 9(a), during no rainfall, the mean value of TROWARA ILW and HATPRO ILW is around 0.08 and 0.2 mm, respectively. TROWARA ILW is close to zero in cloudless conditions, while it is around 0.1 mm for HATPRO. This confirms the fact that HATPRO retrievals overestimate ILW. During rainfall, TROWARA ILW and HATPRO ILW increase dramatically. As shown in Fig. 9(b), HATPRO ILW is significantly overestimated compared to TROWARA ILW. The slope and intercept of the linear fit are 1.63 and −0.1 mm, respectively. The area with the minimum distribution density (light blue area) corresponds to large values of HATPRO ILW, and the linear regression fit line is located above the 1:1 line. TROWARA ILW and HATPRO ILW also present similar variations. The R^2 and RMSE between TROWARA and HATPRO ILW are 0.81 and 0.27 mm, respectively.

The overestimation of HATPRO IWV and ILW could be due to the fact that Tb in the K-band observed by the HATPRO radiometer is overestimated, e.g., in the 22-GHz channel. We simply adjusted the brightness temperature of HATPRO by a constant difference from RTSE and reretrieved the IWV. Although the bias in IWV was slightly reduced, the overestimation persisted. Therefore, the retrieval method itself may be the main contributing factor to the overestimation of

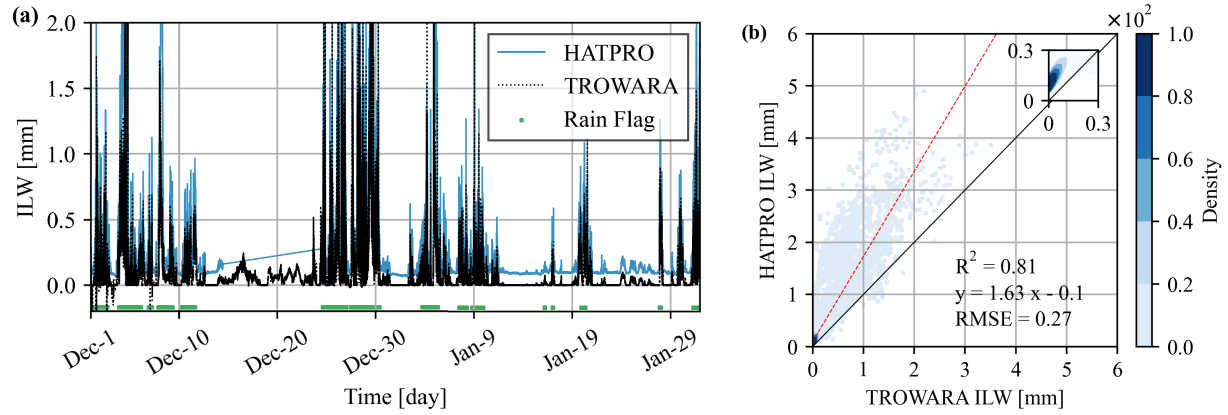

Fig. 9. (a) Time series of the ILW provided by HATPRO and TROWARA from December 1, 2021 to January 31, 2022. The rain flag data observed by the HATPRO rain detector are used to identify rain. (b) Scatter plot of ILW provided by HATPRO and TROWARA from December 1, 2021 to January 31, 2022. The black solid line is the 1:1 line, and the red dashed line is the linear regression fit line. The blue gradient represents the density of the scatter distribution calculated by the Gaussian kernel. The subplot is the ILW scatter plot from 0 to 0.3 mm.

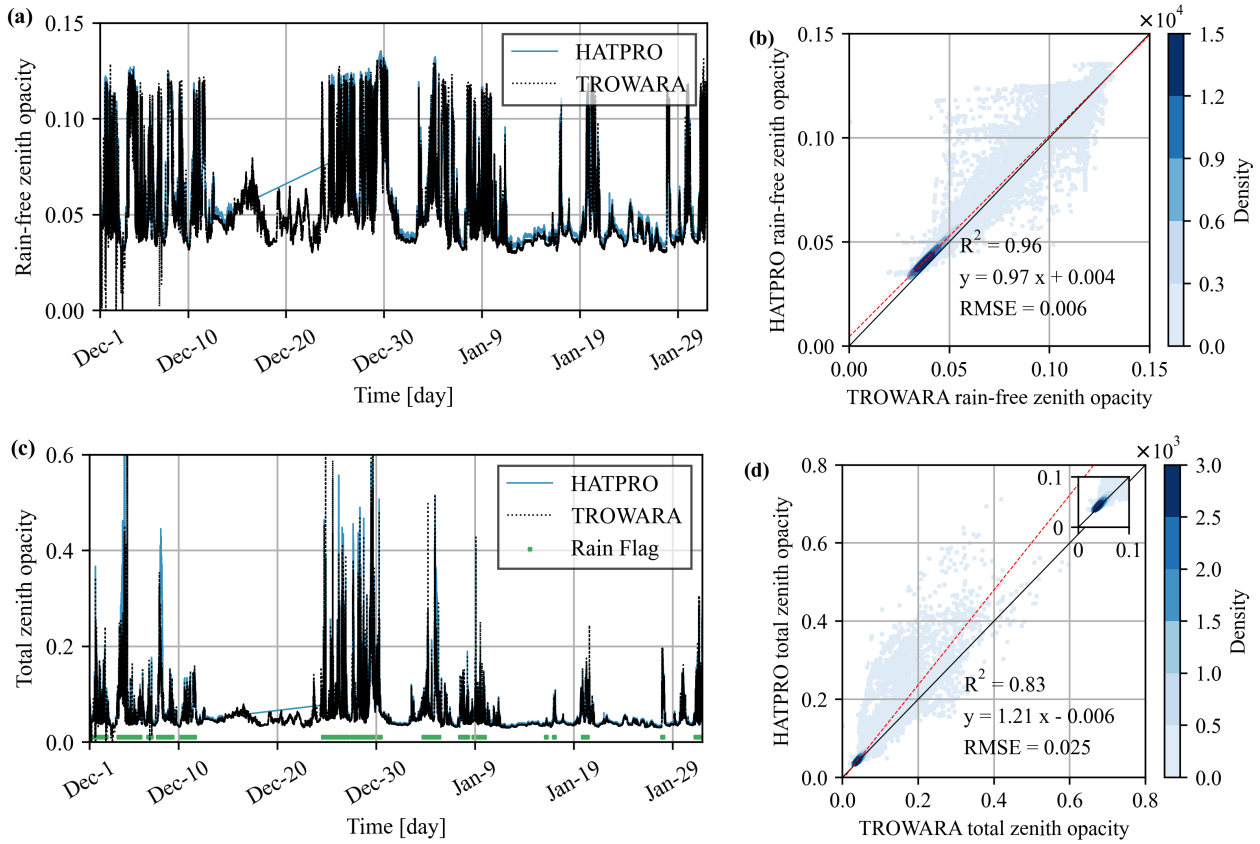

Fig. 10. (a) Time series of the rain-free zenith opacity provided by HATPRO and TROWARA from December 1, 2021 to January 31, 2022. (b) Scatter plot of the rain-free zenith opacity provided by HATPRO and TROWARA from December 1, 2021 to January 31, 2022. The black solid line is the 1:1 line, and the red dashed line is the linear regression fit line. The blue gradient represents the density of the scatter distribution calculated by the Gaussian kernel. (c) Time series of the total zenith opacity provided by HATPRO and TROWARA from December 1, 2021 to January 31, 2022. The rain flag data observed by the HATPRO rain detector are used to identify rain. (d) Scatter plot of the total zenith opacity provided by HATPRO and TROWARA from December 1, 2021 to January 31, 2022. The black solid line is the 1:1 line, and the red dashed line is the linear regression fit line. The blue gradient represents the density of the scatter distribution calculated by the Gaussian kernel. The subplot is the ILW scatter plot from 0 to 0.1.

IWV. Rose et al. [26] indicated limitations of the HATPRO G2 retrieval methods. The relationship between atmospheric water and brightness temperature varies by region and season, and statistical algorithms are problematic in a wide range of applications. This weakness of the HATPRO QR affects the retrieval accuracy of IWV and ILW. As we show in the following, another cause leading to the overestimation of IWV and ILW by HATPRO is the water film on the radome during and shortly after rain events.

Opacities are used for rain rate retrieval at 31 GHz and to study the effect of water on the radome. Fig. 10 shows a two-month time series and scatter plot of the rain-free zenith opacity and total zenith opacity (both rain-free zenith opacity and rain zenith opacity). HATPRO opacity is not calculated using the attenuation retrieved from the HATPRO QR, but by (4) and (10) in the same way as TROWARA. Note that the rain-free zenith opacity during rainfall is not provided by radiometers but is obtained by interpolating before and after

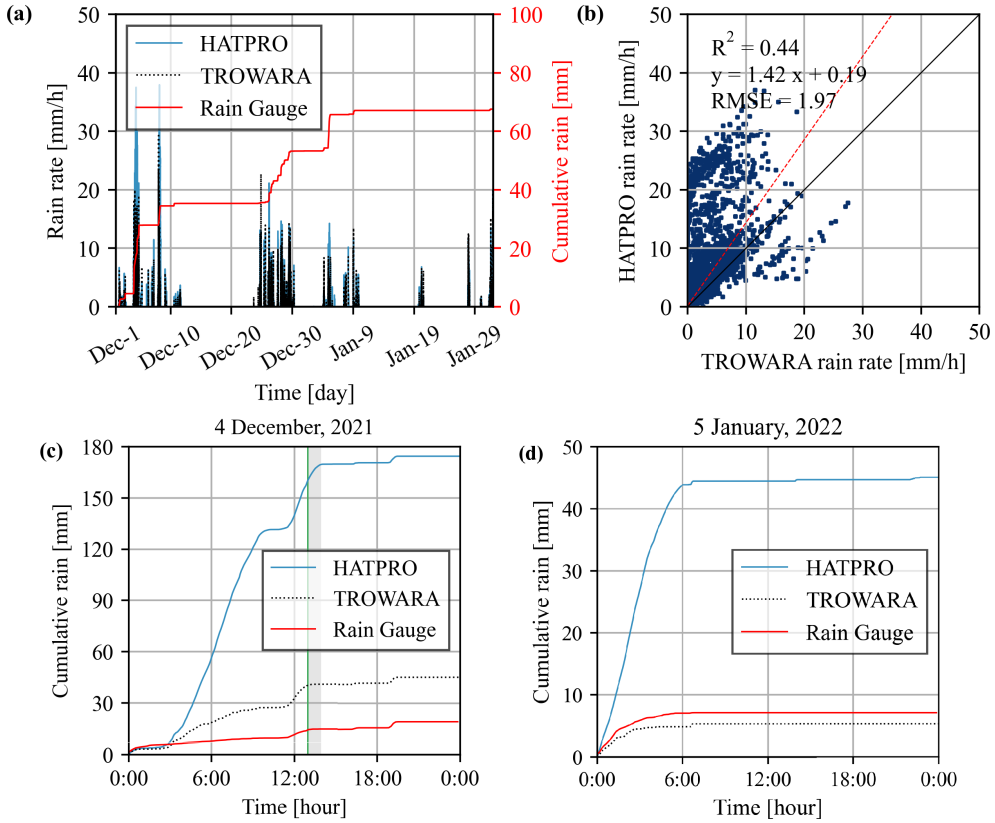

Fig. 11. (a) Time series of rain rates provided by HATPRO, TROWARA, and rain gauge from December 1, 2021 to January 31, 2022. (b) Scatter plot of rain rates provided by HATPRO and TROWARA from December 1, 2021 to January 31, 2022. The solid black line is the 1:1 line, and the red dashed line is the linear regression fit line. (c) Cumulative rain lines provided by HATPRO, TROWARA, and rain gauge on December 4, 2021. The time for the green line is 12:58 UT. The shaded area is from 12:58 UT to 13:55 UT. (d) Cumulative rain provided lines by HATPRO, TROWARA, and rain gauge on January 5, 2022.

rain. There is a high possibility of raindrops in the atmosphere if the ILW value is greater than or equal to 0.4 mm [18], [45], so ILW = 0.4 mm is used as the rainfall threshold for TROWARA. The ILW threshold for rainfall is usually between 0.1 and 0.6 mm. In fact, even if the threshold is not as accurate, the detection of rain occurrence is sufficient. This is because the enhanced emission due to the Mie effect leads to a very strong increase in ILW when the droplet size (diameter) increases to 0.3 mm. Since HATPRO retrieved a higher ILW as previously described, the threshold for rainfall is set to 0.6 mm. As shown in Fig. 10(a) and (b), during no rainfall, the HATPRO zenith opacity agrees well with TROWARA zenith opacity. The slope and intercept of the linear fit are 0.97 and 0.004, respectively. The zenith opacity of TROWARA and HATPRO also presents the same variations. The R^2 and RMSE between TROWARA and HATPRO zenith opacity are 0.96 and 0.006, respectively. As shown in Fig. 10(c) and (d), during rainfall, HATPRO zenith opacity is overestimated compared to TROWARA zenith opacity. The slope and intercept of the linear fit are 1.21 and −0.006, respectively. The linear regression fit line is located above the 1:1 line. On the other hand, the zenith opacity of TROWARA and HATPRO presents similar variations. The R^2 and RMSE between TROWARA and HATPRO zenith opacity are 0.83 and 0.025, respectively.

Fig. 11(a) and (b) shows a two-month time series and scatter plot of rain rates retrieved by (11) at 31 GHz. The rain gauge data are from the ExWi weather station with a time resolution of 10 min. As shown in Fig. 11(a), HATPRO and TROWARA are very consistent in determining the occurrence/duration of rainfall. The more rain is measured by the rain gauge, the higher the estimated rain rate for HATPRO and TROWARA are. Note that HATPRO and TROWARA detect rain, but the rain gauge does not measure any rain, such as December 5 and 6 and January 19 and 20. This may be due to two reasons. First, the time resolution of HATPRO and TROWARA is high so that rain detected for a particularly short time contributes very little to the cumulative rain. Second, virga rainfall evaporates or sublimates before reaching the ground [46]. As shown in Fig. 11(b), HATPRO rain rates are significantly overestimated compared to TROWARA rain rates. Some smaller values (less than 10 mm/h) of TROWARA rain rates correspond to larger values (15–40 mm/h) of HATPRO rain rates. The slope and intercept of the linear fit are 1.42 and 0.19 mm/h, respectively. The linear regression fit line is located above the 1:1 line, and HATPRO rain rates agree poorly with TROWARA rain rates. The R^2 and RMSE between TROWARA and HATPRO rain rates are 0.44 and 1.97 mm/h, respectively. Fig. 11(c) and (d) shows the cumulative rain versus time for the heavy and moderate rain cases, respectively. Cumulative rain of TROWARA presents similar variations to rain gauge cumulative rain, but HATPRO continues to increase after TROWARA and rain gauge stop increasing, such as from 12:58 UT to 13:55 UT. As shown in Fig. 11(c), during heavy rain, both HATPRO and TROWARA cumulative rain

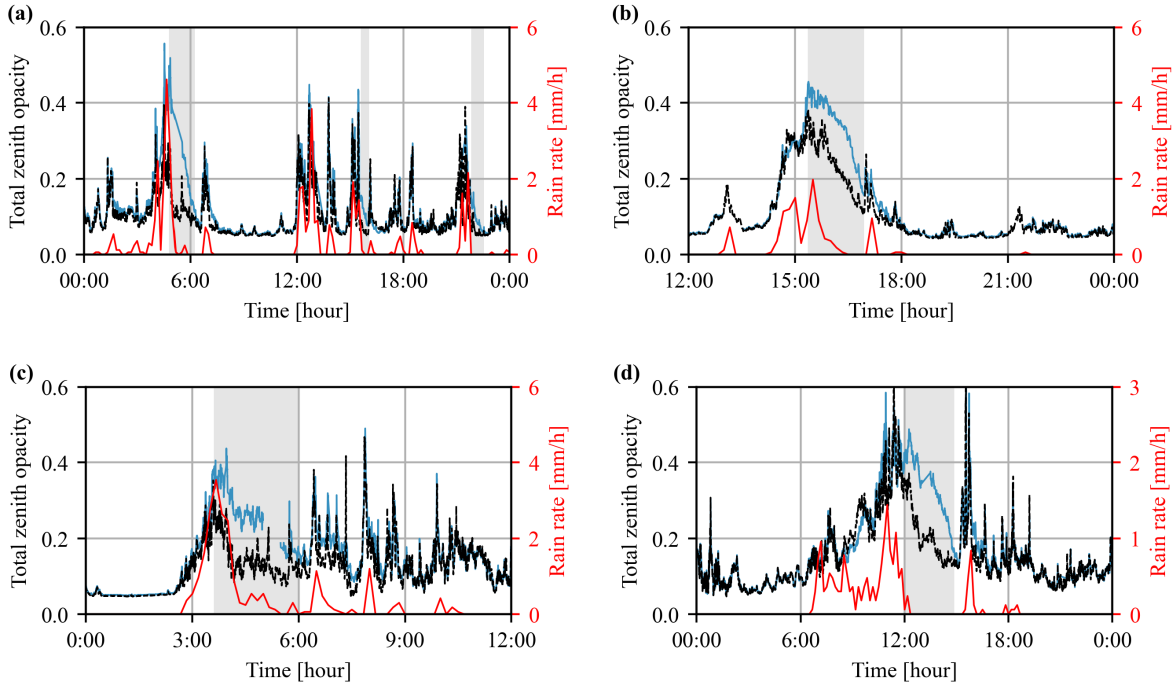

Fig. 12. Time series of total zenith opacity provided by HATPRO (blue solid line) and TROWARA (black dashed line), as well as rain rates measured by rain gauge in (a) December 26, 2021; (b) December 27, 2021; (c) December 28, 2021; and (d) December 29, 2021. The shaded area marks when the zenith opacity of HATPRO is much stronger than that of TROWARA.

are overestimated compared to rain gauge cumulative rain. HATPRO is heavily overestimated to about nine times the rain gauge values. As shown in Fig. 11(d), during moderate rain, the TROWARA cumulative rain agrees relatively well with rain gauge cumulative rain, as described by Wang et al. [19], but HATPRO is heavily overestimated to about six times the rain gauge values.

We used the same rain zenith opacity algorithm for HATPRO and TROWARA at 31 GHz, but HATPRO shows a significant rainfall overestimation. One of the reasons is that the radome of the HATPRO radiometer placed outdoors is contaminated with liquid water left on it by rainfall. This situation can exist during and after rain. Fig. 12 shows the examples of total zenith opacity for HATPRO and TROWARA with rain. The rain rate decreases or stops, while the total zenith opacity of HATPRO remains very strong, such as on December 26 from 4:32 UT to 6:34 UT, December 27 from 15:22 UT to 16:57 UT, December 28 from 3:34 UT to 5:42 UT, and December 29 from 11:52 UT to 15:08 UT. The HATPRO zenith opacity is significantly higher than TROWARA by a maximum of 0.2. There are also some cases with less impact on HATPRO zenith opacity, such as on December 26 from 15:31 UT to 16:01 UT and 21:45 UT to 22:47 UT. When the removal of the water film is effective, the HATPRO zenith opacity agrees very well with TROWARA. This shows that for outdoor radiometers, the blower and hydrophobic coating play a role too.

V. Conclusion

The commercial radiometer HATPRO G2 is widely used as a source of information on atmospheric water parameters important to climate change research. To explore the bias of measurements and the uncertainty of atmospheric water retrievals of HATPRO, we compared it with a radiometer TROWARA with the same observation principle but different instrument characteristics for indoor and outdoor parallel observations. The dataset contains more than 981 000 observations over a 62-day period from December 1, 2021 to January 31, 2022, during various weather conditions. TROWARA brightness temperatures agree well with RTSE, but there is a significant difference between brightness temperature measurements from HATPRO and TROWARA. HATPRO has the largest overestimation at 22.24 GHz, about 5 K, and the minimum overestimation at 31.4 GHz, about 1 K. Their retrieved IWV and ILW present similar changes, with R^2 of 0.84 and 0.81, respectively. IWV and ILW retrieved from HATPRO are significantly overestimated using the QR retrieval method compared to TROWARA, with slopes of 1.73 and 1.63, respectively. Since the outdoor operation of HATPRO has liquid water on the radome during and after rain, its retrieval of rain rates is less than satisfactory. Nevertheless, rain-free opacity calculated by HATPRO at 31.4 GHz using the radiative transfer equation is in good agreement with TROWARA. The R^2 and slope are 0.96 and 0.97, respectively.

To explore the causes of the brightness temperature bias in HATPRO and TROWARA at 22 GHz, we use the GBDT to compare the importance of factors to the bias. The results show that the instrument calibration, instrument surrounding environment, and Sun elevation angle have major contributions to the bias. The determination of the main contributing factors can help to further establish correction models and optimize the instrument.

TROWARA is possibly the sole indoor radiometer in the world that can measure tropospheric water parameters during rainfall. Our study showed that an indoor radiometer has many advantages since it does not affect the microwave radiation

due to the water film on the radome. It would be desirable to install more indoor radiometers for weather observations in the future so that rainfall events can be better accessed and mobile outdoor radiometers can be cross-validated.

ACKNOWLEDGMENT

The authors thank Christian Mätzler for the software and algorithm support that enabled the Humidity And Temperature PROfiler radiometer (HATPRO) to perform the rain rate retrieval, as well as discussions and improvements of this article. Wenyue Wang thanks Alistair Bell, Renaud Matthey, and Roland Albers for discussions related to the present work.

REFERENCES

[1] D. Ji, J. Shi, H. Letu, W. Li, H. Zhang, and H. Shang, "A total precipitable water product and its trend analysis in recent years based on passive microwave radiometers," *IEEE J. Sel. Topics Appl. Earth Observ. Remote Sens.*, vol. 14, pp. 7324–7335, 2021.

[2] R. Nandan, M. V. Ratnam, V. R. Kiran, and D. N. Naik, "Retrieval of cloud liquid water path using radiosonde measurements: Comparison with MODIS and ERA5," *J. Atmos. Solar-Terr. Phys.*, vol. 227, Jan. 2022, Art. no. 105799.

[3] W. Wang and K. Hocke, "Atmospheric effects and precursors of rainfall over the Swiss Plateau," *Remote Sens.*, vol. 14, no. 12, p. 2938, Jun. 2022.

[4] K. Hocke, L. Bernet, J. Hagen, A. Murk, M. Renker, and C. Mätzler, "Diurnal cycle of short-term fluctuations of integrated water vapour above Switzerland," *Atmos. Chem. Phys.*, vol. 19, no. 19, pp. 12083–12090, Sep. 2019.

[5] E. Sauvageat et al., "Comparison of three high resolution real-time spectrometers for microwave ozone profiling instruments," *IEEE J. Sel. Topics Appl. Earth Observ. Remote Sens.*, vol. 14, pp. 10045–10056, 2021.

[6] L. Bernet et al., "Trends of atmospheric water vapour in Switzerland from ground-based radiometry, FTIR and GNSS data," *Atmos. Chem. Phys.*, vol. 20, no. 19, pp. 11223–11244, Oct. 2020.

[7] J. Judge, J. F. Galantowicz, and A. W. England, "A comparison of ground-based and satellite-borne microwave radiometric observations in the Great Plains," *IEEE Trans. Geosci. Remote Sens.*, vol. 39, no. 8, pp. 1686–1696, Aug. 2001.

[8] J. B. Snider, F. O. Guiraud, and D. C. Hogg, "Comparison of cloud liquid content measured by two independent ground-based systems," *J. Appl. Meteorol.*, vol. 19, no. 5, pp. 577–579, May 1980.

[9] S. Steinke et al., "Assessment of small-scale integrated water vapour variability during HOPE," *Atmos. Chem. Phys.*, vol. 15, no. 5, pp. 2675–2692, Mar. 2015.

[10] D. Cimini, E. R. Westwater, Y. Han, and S. J. Keihm, "Accuracy of ground-based microwave radiometer and balloon-borne measurements during the WVIOP 2000 field experiment," *IEEE Trans. Geosci. Remote Sens.*, vol. 41, no. 11, pp. 2605–2615, Nov. 2003.

[11] A. Foth, H. Baars, P. Di Girolamo, and B. Pospichal, "Water vapour profiles from Raman LiDAR automatically calibrated by microwave radiometer data during HOPE," *Atmos. Chem. Phys.*, vol. 15, no. 14, pp. 7753–7763, Jul. 2015.

[12] M. J. Tauc, D. W. Riesland, L. M. Eshelman, W. Nakagawa, and J. A. Shaw, "Simulations and experimental results of cloud thermodynamic phase classification with three SWIR spectral bands," *J. Appl. Remote Sens.*, vol. 13, no. 3, p. 034526, 2019.

[13] S. Crewell and U. Löhnert, "Accuracy of cloud liquid water path from ground-based microwave radiometry 2. Sensor accuracy and synergy," *Radio Sci.*, vol. 38, no. 3, pp. 1–7, 2003.

[14] A. Bell et al., "W-band radar observations for fog forecast improvement: An analysis of model and forward operator errors," *Atmos. Meas. Techn.*, vol. 14, no. 7, pp. 4929–4946, Jul. 2021.

[15] *High-Precision Microwave Radiometers for Continuous Atmospheric Profiling*. Accessed: Jul. 19, 2022. [Online]. Available: https://www.radiometer-physics.de/download/PDF/Radiometers/HATPRO/

[16] J. Morland, M. C. Coen, K. Hocke, P. Jeannet, and C. Mätzler, "Tropospheric water vapour above Switzerland over the last 12 years," *Atmos. Chem. Phys.*, vol. 9, no. 16, pp. 5975–5988, Aug. 2009.

[17] K. Hocke, N. Kämpfer, C. Gerber, and C. Mätzler, "A complete long-term series of integrated water vapour from ground-based microwave radiometers," *Int. J. Remote Sens.*, vol. 32, no. 3, pp. 751–765, Feb. 2011.

[18] F. Cossu, K. Hocke, A. Martynov, O. Martius, and C. Mätzler, "Atmospheric water parameters measured by a ground-based microwave radiometer and compared with the WRF model," *Atmos. Sci. Lett.*, vol. 16, no. 4, pp. 465–472, Oct. 2015.

[19] W. Wang, K. Hocke, and C. Mätzler, "Physical retrieval of rain rate from ground-based microwave radiometry," *Remote Sens.*, vol. 13, no. 11, p. 2217, Jun. 2021.

[20] D. Cimini, T. J. Hewison, and L. Martin, "Comparison of brightness temperatures observed from ground-based microwave radiometers during TUC," *Meteorologische Zeitschrift*, vol. 15, no. 1, pp. 19–26, 2006.

[21] V. Mattioli, E. Westwater, and V. Morris, "Monitoring of precipitable water vapor and cloud liquid path from scanning microwave radiometers during the 2003 cloudiness inter-comparison experiment," in *Proc. 14th ARM Sci. Team Meeting*, Mar. 2004, pp. 1–10.

[22] V. Mattioli, E. R. Westwater, S. I. Gutman, and V. R. Morris, "Forward model studies of water vapor using scanning microwave radiometers, global positioning system, and radiosondes during the cloudiness intercomparison experiment," *IEEE Trans. Geosci. Remote Sens.*, vol. 43, no. 5, pp. 1012–1021, May 2005.

[23] F. S. Marzano, D. Cimini, and R. Ware, "Monitoring of rainfall by ground-based passive microwave systems: Models, measurements and applications," *Adv. Geosci.*, vol. 2, pp. 259–265, Jul. 2005.

[24] F. S. Marzano, D. Cimini, P. Ciotti, and R. Ware, "Modeling and measurement of rainfall by ground-based multispectral microwave radiometry," *IEEE Trans. Geosci. Remote Sens.*, vol. 43, no. 5, pp. 1000–1011, May 2005.

[25] R. Ware, D. Cimini, P. Herzegh, F. Marzano, J. Vivekanandan, and E. Westwater, "Ground-based microwave radiometer measurements during precipitation," in *Proc. 8th Spec. Meeting Microw. Radiometry*, 2004, pp. 24–27.

[26] T. Rose, S. Crewell, U. Löhnert, and C. Simmer, "A network suitable microwave radiometer for operational monitoring of the cloudy atmosphere," *Atmos. Res.*, vol. 75, no. 3, pp. 183–200, May 2005.

[27] S. A. Buehler, J. Mendrok, P. Eriksson, A. Perrin, R. Larsson, and O. Lemke, "ARTS, the atmospheric radiative transfer simulator—Version 2.2, the planetary toolbox edition," *Geosci. Model Develop.*, vol. 11, no. 4, pp. 1537–1556, 2018.

[28] C. Mätzler and J. Morland, "Refined physical retrieval of integrated water vapor and cloud liquid for microwave radiometer data," *IEEE Trans. Geosci. Remote Sens.*, vol. 47, no. 6, pp. 1585–1594, Jun. 2009.

[29] J. Morland, "TROWARA-tropospheric water vapour radiometer: Radiometer review and new calibration model," Institut für Angew. Physik, Universität Bern, Bern, Switzerland, IAP Res. Rep., 2002-15-MW 2002.

[30] R. Peter and N. Kämpfer, "Radiometric determination of water vapor and liquid water and its validation with other techniques," *J. Geophys. Res., Atmos.*, vol. 97, no. D16, pp. 18173–18183, 1992.

[31] J. Morland, "TROWARA-Rain flag development and stability of instrument and calibration," Institut für Angew. Physik, Universität Bern, Bern, Switzerland, IAP Res. Rep. 2007-13-MW, 2007.

[32] F. Navas-Guzmán, N. Kämpfer, and A. Haefele, "Validation of brightness and physical temperature from two scanning microwave radiometers in the 60 GHz O_2 band using radiosonde measurements," *Atmos. Meas. Techn.*, vol. 9, no. 9, pp. 4587–4600, 2016.

[33] *Radiometer Physics GmbH*. Accessed: Jul. 19, 2022. [Online]. Available: http://www.radiometer-physics.de

[34] S. Kazama, T. Rose, R. Zimmermann, and R. Zimmermann, "A precision autocalibrating 7 channel radiometer for environmental research applications," *J. Remote Sens. Soc. Jpn.*, vol. 19, no. 3, pp. 265–273, 1999.

[35] Y. Han and E. R. Westwater, "Analysis and improvement of tipping calibration for ground-based microwave radiometers," *IEEE Trans. Geosci. Remote Sens.*, vol. 38, no. 3, pp. 1260–1276, May 2000.

[36] J. Hu et al., "Characterization of brightness temperature biases at channels 13 and 14 for FY-3C MWHS-2," *IEEE Trans. Geosci. Remote Sens.*, vol. 60, pp. 1–14, 2021.

[37] N. Zhang et al., "Forest height mapping using feature selection and machine learning by integrating multi-source satellite data in Baoding city, North China," *Remote Sens.*, vol. 14, no. 18, p. 4434, Sep. 2022.

[38] J. H. Friedman, "Greedy function approximation: A gradient boosting machine," *Ann. Statist.*, vol. 29, no. 5, pp. 1189–1232, Oct. 2001.

[39] *Operation Principles and Software Description for Rpg Standard Single Polarization Radiometers*. Accessed: Jul. 19, 2022. [Online]. Available: https://www.radiometer-physics.de/download/PDF/Radiometers/HATPRO/

[40] K. Hocke, L. Bernet, W. Wang, C. Mätzler, M. Hervo, and A. Haefele, "Integrated water vapor during rain and rain-free conditions above the Swiss Plateau," *Climate*, vol. 9, no. 7, p. 105, Jun. 2021.

[41] H. J. Liebe, M. C. Thompson, and T. A. Dillon, "Dispersion studies of the 22 GHz water vapor line shape," *J. Quant. Spectrosc. Radiat. Transf.*, vol. 9, no. 1, pp. 31–47, Jan. 1969.

[42] V. Meunier, U. Löhnert, P. Kollias, and S. Crewell, "Biases caused by the instrument bandwidth and beam width on simulated brightness temperature measurements from scanning microwave radiometers," *Atmos. Meas. Techn.*, vol. 6, no. 5, pp. 1171–1187, May 2013.

[43] C. Straub, A. Murk, and N. Kämpfer, "MIAWARA-C, a new ground based water vapor radiometer for measurement campaigns," *Atmos. Meas. Techn.*, vol. 3, no. 5, pp. 1271–1285, Sep. 2010.

[44] M. Hervo, P. Bättig, and A. Haefele, "Evaluation of the new microwave radiometer HATPRO-G5," Eidgenössisches Departement des Innern EDI, Bundesamt für Meteorologie und Klimatologie MeteoSchweiz, Payerne, Switzerland, Res. Rep., 2021.

[45] U. Löhnert and S. Crewell, "Accuracy of cloud liquid water path from ground-based microwave radiometry 1. Dependency on cloud model statistics," *Radio Sci.*, vol. 38, no. 3, p. 8041, 2003.

[46] R. Beynon and K. Hocke, "Snow virga above the Swiss Plateau observed by a micro rain radar," *Remote Sens.*, vol. 14, no. 4, p. 890, Feb. 2022.

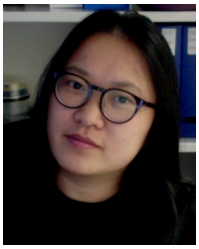

Wenyue Wang received the M.Sc.(Eng.) degree in cartography and geographical information engineering from the China University of Mining and Technology, Xuzhou, China, in 2019. She is currently pursuing the Ph.D. degree in climate sciences with the University of Bern, Bern, Switzerland.

Her research interests include microwave remote sensing, atmospheric water detected from ground-based microwave radiometer, estimation of rain rate, and the study of rainfall precursors and nowcasting.

Axel Murk received the M.Sc. degree in physics from the Technical University of Munich, Munich, Germany, in 1995, and the Ph.D. degree in physics from the University of Bern, Bern, Switzerland, in 1999.

He is currently the Leader of the Microwave Physics Division, Institute of Applied Physics, University of Bern. He has been involved in the development and characterization of millimeter- and submillimeter-wave instrumentation for different ground-based and space-borne projects. His research interests include digital real-time spectrometers and the radiometric calibration of remote sensing instruments.

Eric Sauvageat received the M.S.(Eng.) degree in energy management and sustainability from the École Polytechnique Fédérale de Lausanne, Lausanne, Switzerland, in 2018. He is currently pursuing the Ph.D. degree in applied physics with the University of Bern, Bern, Switzerland.

His main research interests include microwave remote sensing and data analysis of atmospheric processes, with a focus on middle-atmospheric ozone.

Wenzhi Fan received the M.Sc.(Eng.) degree in photogrammetry and remote sensing from the China University of Mining and Technology, Xuzhou, China, in 2019. He is currently pursuing the Ph.D. degree in geophysics with Peking University, Beijing, China.

His main research interests include research in large-scale synthetic aperture radar (SAR) interferometry and applications to surface loading.

Christoph Dätwyler received the M.Sc. degree in mathematics from the Eidgenössische Technische Hochschule Zürich, Zürich, Switzerland, in 2014, and the Ph.D. degree in climate sciences from the University of Bern, Bern, Switzerland, in 2019.

His research interests include atmospheric physics.

Maxime Hervo currently works at the Federal Office of Meteorology and Climatology, MeteoSwiss, Payerne, Switzerland. His research interests include atmospheric physics.

Alexander Haefele received the M.S. and Ph.D. degrees from the University of Bern, Bern, Switzerland, in 2005 and 2009, respectively.

He currently works at the Federal Office of Meteorology and Climatology, MeteoSwiss, Payerne, Switzerland.

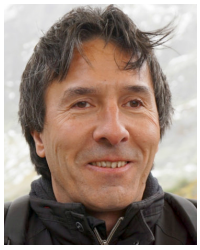

Klemens Hocke received the Venia Legendi in atmospheric physics from the University of Bern, Bern, Switzerland, in 2011.

He is currently the Leader of the Atmospheric Processes Group, Institute of Applied Physics, University of Bern. His research interests include atmospheric dynamics, remote sensing, and data analysis of atmospheric water and stratospheric ozone.